

# Earth's Future

## RESEARCH ARTICLE

10.1029/2021EF002598

# Increased Radon Exposure From Thawing of Permafrost Due To Climate Change

P. W. J. Glover<sup>1</sup>  and M. Blouin<sup>2</sup>

<sup>1</sup>School of Earth and Environment, University of Leeds, Leeds, UK, <sup>2</sup>Geostack, Québec, QC, Canada

### Key Points:

- Permafrost acts as a radon barrier, reducing radiation to a tenth of the background level, and increasing it behind the barrier
- Instantaneous thawing gives plumes >200 Bq/m<sup>3</sup> for over 5 years in buildings with basements, but no increase in pile-supported buildings
- Radiation plumes over 200 Bq/m<sup>3</sup> for up to 4 years also occur when slower thawing that results in 40% thaw in less than 15 years is modeled

### Correspondence to:

P. W. J. Glover,  
[p.w.j.glover@leeds.ac.uk](mailto:p.w.j.glover@leeds.ac.uk)

### Citation:

Glover, P. W. J., & Blouin, M. (2022). Increased radon exposure from thawing of permafrost due to climate change. *Earth's Future*, 10, e2021EF002598. <https://doi.org/10.1029/2021EF002598>

Received 9 DEC 2021  
Accepted 21 JAN 2022

### Author Contributions:

**Conceptualization:** P. W. J. Glover  
**Data curation:** P. W. J. Glover  
**Formal analysis:** P. W. J. Glover, M. Blouin  
**Investigation:** P. W. J. Glover, M. Blouin  
**Methodology:** P. W. J. Glover, M. Blouin  
**Project Administration:** P. W. J. Glover  
**Resources:** P. W. J. Glover  
**Supervision:** P. W. J. Glover  
**Validation:** P. W. J. Glover, M. Blouin  
**Visualization:** P. W. J. Glover  
**Writing – original draft:** P. W. J. Glover  
**Writing – review & editing:** P. W. J. Glover

© 2022 The Authors. Earth's Future published by Wiley Periodicals LLC on behalf of American Geophysical Union. This is an open access article under the terms of the [Creative Commons Attribution-NonCommercial-NoDerivs License](https://creativecommons.org/licenses/by-nc-nd/4.0/), which permits use and distribution in any medium, provided the original work is properly cited, the use is non-commercial and no modifications or adaptations are made.

**Abstract** Radon is a natural radioactive gas accounting for approximately one in 10 lung cancer deaths, with substantially higher death rates in sub-Arctic communities. Radon transport is significantly reduced in permafrost, but permafrost is now thawing due to climate change. The effect of permafrost thawing on domestic radon exposure is unknown. Here we present results from radon transport modeling through soil, permafrost, and model buildings either with basements or built on piles. We find that permafrost acts as an effective radon barrier, reducing radiation exposure to a tenth of the background level while producing a ten-fold increase in the radon activity behind the barrier. When we model thawing of the permafrost barrier, we find no increase in radon to the background level for buildings on piles. However, for buildings with basements, the radon increases to over one hundred times its initial value and can remain above the 200 Bq/m<sup>3</sup> threshold for up to 7 years depending on the depth of the permafrost and the speed of thawing. When thawing speed is taken into account, radiations remain higher than the threshold for all scenarios where 40% thawing occurs within 15 years. This new information suggests that a significant sub-Arctic population could be exposed to radon levels dangerous to health as a result of climate change thawing of permafrost, with implications for health provision, building codes, and ventilation advice.

**Plain Language Summary** Radon is an invisible natural radioactive gas that causes approximately one in 10 lung cancer deaths. It affects smokers much more than non-smokers and causes higher death rates in sub-Arctic communities. Radon flow is significantly reduced by permafrost, but permafrost is now thawing due to climate change. This paper models flow of radon through the soil, permafrost, and model buildings either with basements or on piles. We find that permafrost acts as an effective radon barrier. It reduces radiation to about a tenth of the background level. The trapped radon produces increased radiation behind the barrier. When we model thawing of the permafrost barrier, we find no increase in radon to the background level for buildings built on piles. However, for buildings with basements, the radon increases to more than one hundred times its initial value for up to 7 years depending on the depth of the permafrost and how fast the permafrost thaws. This new information suggests that a significant sub-Arctic population could be exposed to radon levels dangerous to health as a result of permafrost thawing due to climate change. This has implications for health provision, building codes, and ventilation advice.

## 1. Introduction

The National Council on Radiation Protection and Measurements has identified naturally occurring radon as the largest source of environmental radiation to persons living in the United States, and the second leading cause of lung cancer after smoking (Dela Cruz et al., 2011; Nitzbon et al., 2020). Radon has been estimated to cause between 8,000 and 45,000 lung cancer deaths per year (Al-Zoughool & Krewski, 2009; Pawel & Puskin, 2003). Radon causes approximately 10%–14% of lung cancer deaths in the USA (BEIR VI, 1999; Krewski et al., 2005; Krewski et al., 2006; Lubin et al., 2004; WHO, 2019) and about 3.3%–8.3% in Europe (Darby et al., 2005, 2006; WHO, 2009).

Radon is produced from rocks and soils containing significant concentrations of U<sup>238</sup> and its decay products (Peto & Darby, 1994). It is transported through the rocks and soils by diffusion and advection (Chen et al., 1995; Othman et al., 2021), ultimately being either dispersed harmlessly in the atmosphere or leaching into buildings through their foundations, where high concentrations can accumulate if the building is not ventilated (Chung et al., 2020). The worldwide average (UNSCEAR, 2000) Ra<sup>226</sup> activity is 39 Bq/kg. The diffusive and advective transport of radon through the soil is controlled by the porosity, fluid saturations, diffusion coefficients, and

relative permeabilities of the soil. All of these parameters are expected to be reduced significantly in permafrost (Fortin et al., 2007).

Since permafrost makes up about one-fifth of the Earth's terrestrial surface (Worsley, 1986), it would be expected that buildings constructed on permafrost might be protected to some degree by the permafrost acting as a radon barrier. It might also be expected that rapid permafrost thawing (Nitzbon et al., 2020), which is now occurring as a result of climate change (Witze, 2020; Yumashev et al., 2019), might expose people living or working in buildings that were once underlain by permafrost to increased concentrations of radon as well as leading to further releases of carbon (Turetsky et al., 2020).

The global cryosphere, defined as all of the areas on Earth with frozen water, shrank on average by about 87,000 km<sup>2</sup> per year (about 33,000 square miles per year), between 1979 and 2016 as a result of climate change according to a recent study (Peng et al., 2021). It has also been recently estimated that 5 million people live on permafrost in the Arctic Circumpolar Permafrost Region (ACPR), of which 42% will become permafrost-free due to climate-driven thawing by 2050, affecting 3.3 million inhabitants (Ramage et al., 2021). The solid geology of these northern polar regions is predominantly composed of metamorphic and plutonic terranes (Petrov & Purbellier, 2018) that contain raised levels of U<sup>238</sup> and its decay products (Scheib et al., 2009), exacerbating the risk.

Sociological factors need also to be taken into account. It is well recognized that radon-acquired lung cancer is about 26 times (25.8 + 5.4/−4.5) more prevalent in tobacco smokers than it is for non-smokers (Darby et al., 2005; Krewski et al., 2006; Lubin et al., 2004). This is especially important considering that the prevalence of smoking in the Arctic has always been high (79% for the Inuit of Greenland in 1997 (Bjerregaard et al., 1997), 62.3% for the Inuit of Canadian Arctic in 2012). The sparsity of data means that more recent estimates are not available, but though likely to be smaller, still considerably higher than recent values of 17.8%, 23%, and 16.3% for the UK, EU, and the USA, respectively (WHO, 2009). It seems that in arctic Canada at least, the population is likely to be more sensitive to increases in domestic and workplace radon as a result of their lifestyle. This may be balanced to some extent by the style of buildings that predominate. In northern areas, it is more common for buildings to be raised off the ground on piles, with natural ventilation occurring below the building (Buijze & Wright, 2021). This type of construction would be naturally immune to radon.

Little is known about the transport of radon in soils and especially in permafrost. In this modeling, we use the best values we can obtain in order to numerically model the transport of radon through the soil and into several types of building, both in the presence of a permafrost layer and when the permafrost has thawed. While radon comes from many sources, not only from rocks and soil containing a large amount of U<sup>238</sup> and its decay products, we have restricted our initial modeling to this source. Consequently, we do not consider radon arising from building materials, pollutants in the atmosphere, water supply, or natural gas used for heating and kitchen equipment. These additional sources may have an impact on radon in some buildings, and hence the data presented in this paper should be considered as a lower bound.

## 2. Methods

### 2.1. The Model

All modeling is carried out by the finite element solution of linked partial differential equations in two dimensions and as a function of time using Comsol Multiphysics®. An example of the physical models used is shown in Figure 1. Each is 60 m wide and includes a 45 m depth of soil. The permafrost layer for each calculation has a uniform thickness, which has been varied between 0.5 and 5 m in 0.5 m steps. The unfrozen topsoil layer has been assumed to be of uniform thickness and has been varied between 0 and 15 m thick in four steps. There are three soil domains: (a) soil below the permafrost layer, (b) the permafrost layer, and (c) the soil above the permafrost layer on each side of the building.

The model buildings are each split into three domains. For the modern building style, the domains are (a) a rectangular basement (18 m wide), which is either just below the surface of the soil and penetrates into the permafrost layer (3 m high) or rests directly on the soil and is 2 m high, (b) a rectangular main living space (10 m high, 18 m wide), and (c) a triangular roof space (5 m high, 18 wide). For the traditional style of building, the domains are (a) a ventilated underfloor space (2 m high, 18 m wide), which contains piles that penetrate into the

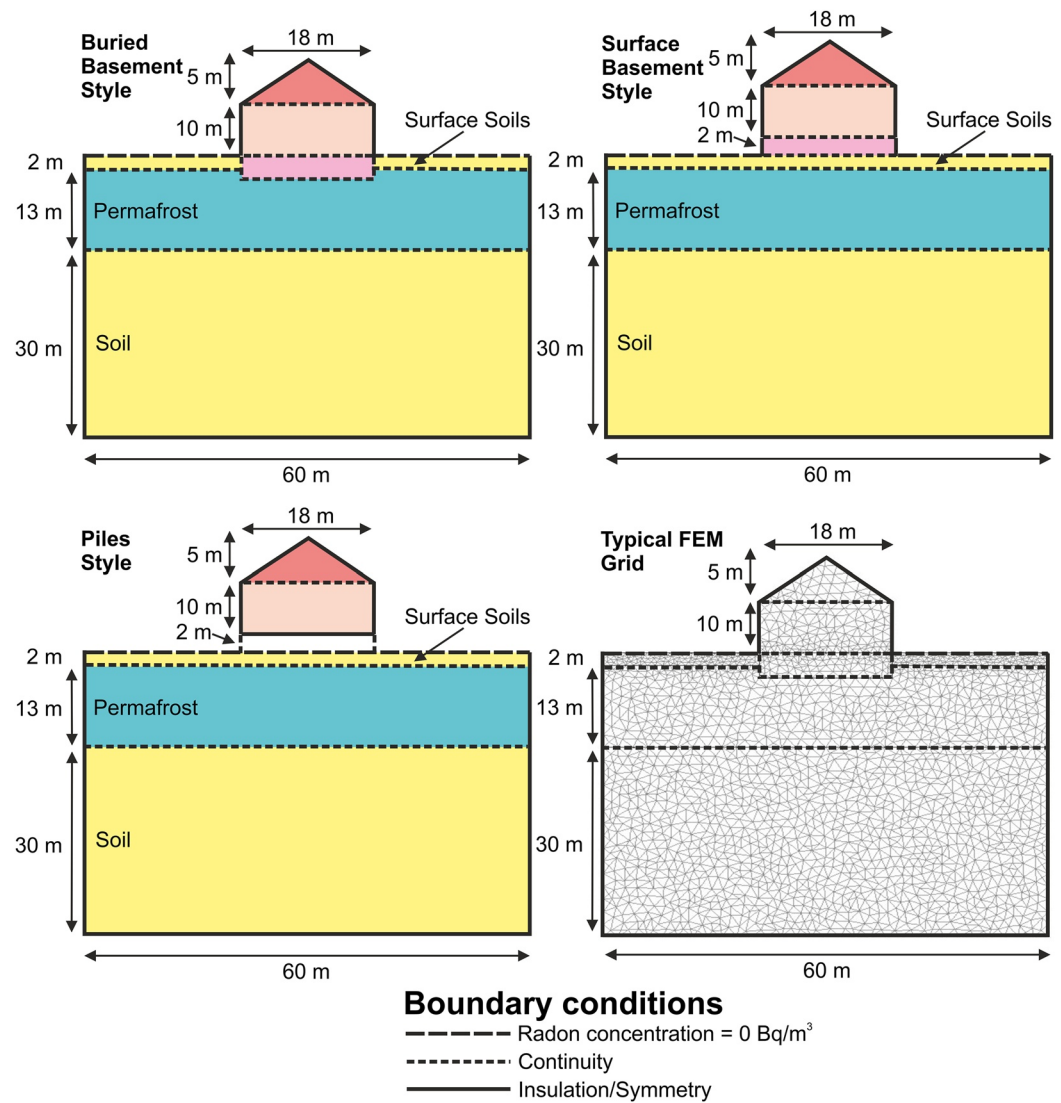


**Figure 1.** The geometries of the three models tested in this work with dimensions and boundary conditions. Top left shows a building with a basement that is buried in the ground. Top right shows essentially the same building but with the whole building resting on the surface of the soil and with the basement having insulated walls. The bottom left panel shows a pile-built construction of the same dimensions, where the bottom layer is a well-ventilated space. The bottom right panel shows a typical Finite Element Modeling (FEM) mesh, in this case for the buried basement example.

permafrost layer, (b) a rectangular main living space (10 m high, 18 m wide), and (c) a triangular roof space (5 m high, 18 m wide).

A two dimensional mesh is created and refined in all domains of the model. The mesh consists of triangles that have side lengths no larger than 1 m in the body of the model, and no larger than 0.2 m along all boundaries except those where the boundary conditions of insulation and symmetry are applied, where they are no larger than 0.5 m. There are about 25,000 elements in the final model. The number of elements controls the speed of the final solution. We found that the solutions were reached within several minutes on a standard 3 GHz laboratory PC, and hence retain the described geometry for clarity even though the model is symmetric and could be reduced to half of its size.

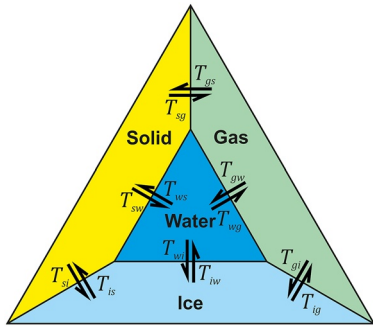


**Figure 2.** Transfer coefficients  $T_{jk} = \alpha_{jk}\Gamma_j C_j$  and their relationship with the four phases present in permafrost.

## 2.2. Differential Equations

This work models radon concentration. Since we are ultimately interested in the radiation that the radon provides, and this radon varies temporally, we do not model radon concentration in atoms per cubic meter or moles per cubic meter, but it becquerels per cubic meter ( $\text{Bq}/\text{m}^3$ ). The becquerel is the SI unit of radiation, where one becquerel (1 Bq) is equal to 1 disintegration per second. Hence modeling is carried out in terms of an effective radiation density provided by the varying radon concentration.

The fundamental differential equations follow from Fick's and Darcy's laws, and Laplace's equation:

$$\bar{J}_{diff,a} = -(1 - S_w) \phi \tau_a D_a \nabla C_a \quad (1)$$

$$\bar{J}_{diff,w} = -S_w \phi \tau_w D_w \nabla C_w \quad (2)$$

$$\bar{J}_{adv,a} = -C_a \frac{k_a}{\mu_a} \nabla P \quad (3)$$

$$\nabla^2 P = 0 \quad (4)$$

where  $J$  is the bulk fluxes of radon ( $\text{Bq m}^{-2} \text{s}^{-1}$ ), the subscripts *adv* and *diff* refer to advection and diffusion respectively, and *a*, *w*, *i*, and *s* refer to air, water, ice, and solid surfaces,  $S_w$  is the water saturation of the pore space (fractional),  $\phi$  is the porosity of the soil (fractional),  $\tau$  are the tortuosities of the radon flow (fractional) in each phase,  $D_w$  and  $D_a$  are the diffusion coefficients of radon in water and air ( $\text{m}^2 \text{s}^{-1}$ ),  $k_a$  is the intrinsic permeability to air ( $\text{m}^2$ ),  $\mu_a$  is the dynamic viscosity of air,  $C_w$  and  $C_a$  are the radon concentrations in each phase ( $\text{Bq m}^{-3}$ ), and  $P$  is the gas pressure (Pa).

It is assumed that radon is generated within the soil and permafrost at a rate  $\Sigma [\text{Bq m}^{-3} \text{s}^{-1}] = \eta \rho_b \lambda C^{Ra226}$ , which is constant in space (i.e., the same in all soils and permafrost and zero elsewhere) and in time (Gadd & Borak, 1995), where  $\eta$  is the sum of the fractional emanation coefficients into the air, water, ice and adsorbed phase ( $\eta = \eta_{\text{air}} + \eta_{\text{water}} + \eta_{\text{ice}} + \eta_{\text{surface}}$ ),  $\rho_b$  is the soil bulk density ( $\text{kg m}^{-3}$ ),  $\lambda$  is the decay constant of radon ( $\text{s}^{-1}$ ) and  $C^{Ra226}$  is the radium-226 activity per unit dry mass ( $\text{Bq kg}^{-1}$ ).

The mass balance equations for each phase (air, water, ice, and solid surfaces, respectively) are:

$$(1 - S_w - S_i) \phi \frac{\partial C_a}{\partial t} = \nabla \cdot ((1 - S_w - S_i) \phi \tau_a D_a \nabla C_a) + \frac{k_a}{\mu_a} \nabla P \cdot \nabla C_a - (1 - S_w - S_i) \phi \lambda C_a + \eta_a \rho_b \lambda C^{Ra226} - \sum_{j \neq a} (T_{aj} - T_{ja}) \quad (5)$$

$$S_w \phi \frac{\partial C_w}{\partial t} = \nabla \cdot (S_w \phi \tau_w D_w \nabla C_w) - S_w \phi \lambda C_w + \eta_w \rho_b \lambda C^{Ra226} - \sum_{j \neq w} (T_{wj} - T_{jw}) \quad (6)$$

$$S_i \phi \frac{\partial C_i}{\partial t} = \nabla \cdot (S_i \phi \tau_i D_i \nabla C_i) - S_i \phi \lambda C_i + \eta_i \rho_b \lambda C^{Ra226} - \sum_{j \neq i} (T_{ij} - T_{ji}) \quad (7)$$

$$\rho_b \frac{\partial C_s}{\partial t} = -\rho_b \lambda C_s + \eta_s \rho_b \lambda C^{Ra226} - \sum_{j \neq s} (T_{sj} - T_{js}) \quad (8)$$

Advection is assumed negligible for the water and ice phases, while both diffusion and advection are assumed to be negligible for the solid phase at the timescales covered by this modeling. Note that the units of  $C_s$  are exceptionally  $\text{Bq kg}^{-1}$ .

The radon will distribute itself between all four phases by sorption and solution. This process is described by transfer coefficients  $T_{jk}$  ( $\text{Bq m}^{-3} \text{s}^{-1}$ ), which are defined as the rate of transfer of radon activity per unit volume from phase  $j$  to phase  $k$ . The first order transfer coefficients are given by  $T_{jk} = \alpha_{jk} \Gamma_j C_j$ , where  $j, k \in \{a, w, i, s\}$ ,  $\alpha_{jk}$  are exchange rates ( $\text{s}^{-1}$ ),  $C_j$  is radon concentration, and  $\Gamma_j$  is a multiplier ( $\Gamma_j = (1 - S_w - S_i) \phi$ ,  $S_w \phi$ ,  $S_i \phi$ , and  $\rho_b$  for  $j = \{a, w, i, s\}$ , respectively). The transfer coefficient is shown schematically in Figure 2. This figure portrays the four phases that are present in the subsurface (solid matrix, ice, water, and gas). Radon can be transferred between

any two of these phases in either direction, where the transfer depends on the chemical efficacy of the transfer, the area of the interface over which the transfer can take place, and the instantaneous concentrations of radon in each phase. The figure shows the general case where there are 6 pairs of transfer coefficients. In reality, some of these processes are much more important than others, the latter of which may be considered to be negligible, allowing Equations 5 to 8 to be simplified significantly.

By assuming that (a) adsorption to wet surfaces or ice is negligible, (b) exchange between water, air, and ice phases occur at a timescale much shorter than those typical of radon transport, and (c) exchange between the air and solid surface adsorbed phase is fast or negligible, it is possible to follow a reduction similar to that by Rogers and Nielson (1991a, 1991b). Water has a much larger affinity to most minerals than radon, so assumption (a) is reasonable. Typical exchange times between air and water are estimated to be between 0.1 and 10 s for water layers 10–100  $\mu\text{m}$  thick, which is considerably shorter than the timescales involved with concentration changes due to diffusion and advection in soils (hours to days), substantiating the second assumption for water and air. As for the degree of adsorption or absorption of radon molecules on ice surfaces, a comparison of the experimentally determined adsorption enthalpy of radon on ice of  $-19.2 \pm 1.6$  kJ/mol (Eichler et al., 2000) with the adsorption enthalpies of radon on other solid-state surfaces, the solution enthalpy of radon in water, and the formation enthalpy of a hypothetical radon clathrate hydrate all show that with high probability radon is adsorbed as a free atom on the ice surface and is not fully coordinated by water dipoles. We can find no data to support assumption (b) for exchange between ice and air or water.

Consequently, the linked partial differential equations reduce to:

$$\gamma \frac{\partial C_a}{\partial t} = \nabla \cdot (D \nabla C_a) + \frac{k_a}{\mu_a} \nabla P \cdot \nabla C_a - \gamma \lambda C_a + \Sigma \quad (9)$$

where:  $\gamma = (1 - S_w - S_i + S_w L_{aw} + S_i L_{ai}) \phi + \rho_b k_a$  is the operating porosity,  $D = ((1 - S_w - S_i) \tau_a D_a + S_w \tau_w D_w L_{aw} + S_i \tau_i D_i L_{ai}) \phi$  is the effective diffusion coefficient, and  $\Sigma = \eta \rho_b \lambda C^{Ra226}$  is the source term.

The parameters  $L_{aw}$  and  $L_{ai}$  are Ostwald coefficients,  $\tau_j$  are tortuosities,  $D_j$  are diffusion coefficients and  $S_j$  denotes phase fraction for each phase. In this work, we set  $C^{Ra226} = 40$  Bq/kg, which is a conservative 33% of the range 10–100 Bq/kg given by Nazaroff (1992) in his review for mean soils in the USA, and  $\eta = 0.2$ , which is cited as typical for soils after compiling emanation coefficients for soils from 13 sources (Nazaroff, 1992). For simplicity, the thawing assumes all ice thaws to water with no change in porosity, which implies that in this model there is no compaction of soil upon thawing nor radon pumping from the compaction process.

We were unable to find diffusion coefficient data for radon in ice. However, observations of diffusion of  $\text{CO}_2$  through ice in the field vary between  $2.45 \times 10^{-10}$   $\text{m}^2/\text{s}$  and  $1.41 \times 10^{-10}$   $\text{m}^2/\text{s}$ , increasing with temperature (Ahn et al., 2008) and between  $1.1 \times 10^{-11}$   $\text{m}^2/\text{s}$  and  $3 \times 10^{-11}$   $\text{m}^2/\text{s}$  at 270 K for diffusion parallel and perpendicular to the  $c$ -axis, respectively (Ikeda-Fukazawa et al., 2004a, 2004b). When we calculate the diffusion coefficient of  $\text{CO}_2$  through water-ice at 270 K using the method of Evans et al. (2018), we obtain  $5.48 \times 10^{-10}$   $\text{m}^2/\text{s}$ , which is higher than the experimental values. The Evans et al. method can also be used to calculate the diffusion coefficient of radon. When this was done, a value of  $3.2 \times 10^{-10}$   $\text{m}^2/\text{s}$  was obtained, which is a factor of 0.583 of the value for  $\text{CO}_2$ , a factor which remains constant with temperature because it depends only on the relative molecular mass of the diffusing species with respect to the material through which it is diffusing. Consequently, the diffusion coefficient of radon can be taken to be about half of that for  $\text{CO}_2$  in the same medium at the same temperature. Consequently, we have assumed that the mean diffusion coefficient of radon in ice at 270K can be represented by a value of  $2 \times 10^{-11}$   $\text{m}^2/\text{s}$ . Since this value is about 32 times less than the diffusion coefficient for radon in water at 293 K, even a large error will be insignificant in the modeling.

### 2.3. Boundary Conditions and Assumptions

The boundary conditions are shown in Figure 1. All vertical soil boundaries were set to insulation/symmetry conditions as was the lower boundary of the model. These boundary conditions ensure that the model is laterally symmetric and constrains radon transport to the vertical near the boundaries. This effectively removes regional-driven radon transport from the model such as water drainage. The outer walls of the building were set to insulation/symmetry for an unventilated building and to  $C_a = 0$  Bq/ $\text{m}^3$  for a fully ventilated building. These conditions ensure that the two extremes of building ventilation can be modeled, one where the radon can only

**Table 1**  
*Modeling Parameters*

	Parameter/Physical Significance	Units	Value before thaw	Value after thaw	Source/Notes
$S_w$	Fraction of porosity containing water	-	0	0.9	Imposed
$S_i$	Fraction of porosity containing ice	-	0.9	0	Imposed
$L_{aw}$	Ostwald coefficient for the air (gas)/water interface	-	0.253	0.253	Ongori et al. (2015)
$L_{ai}$	Ostwald coefficient for the air (gas)/ice interface	-	0.253	0.253	Assumed = $L_{aw}$
$\Phi$	Porosity (as a fraction)	-	0.245	0.245	Assuming thawing occurs with no compaction
$\rho_b$	Bulk density of the material	kg/m <sup>3</sup>	$2.22 \times 10^3$	$2.25 \times 10^3$	Calculated with $\rho_{ma} = 2,650$ kg/m <sup>3</sup>
$k_a$	Intrinsic permeability of the material to air (gas)	m <sup>2</sup>	$9.87 \times 10^{-17}$	$9.87 \times 10^{-20}$	Chuvilin et al. (2021)
$\tau_a$	Tortuosity of the air (gas) fraction in the pores	-	7	7	Moldrup et al. (2000)
$\tau_i$	Tortuosity of the ice fraction in the pores	-	1	7	Moldrup et al. (2000)
$\tau_w$	Tortuosity of the water fraction in the pores	-	7	1	Moldrup et al. (2000)
$D_{air}$	Diffusion coefficient of radon in air	m <sup>2</sup> s <sup>-1</sup>	$1.1 \times 10^{-5}$	$1.1 \times 10^{-5}$	Barrio-Parra et al. (2022)
$D_i$	Diffusion coefficient of radon in ice	m <sup>2</sup> s <sup>-1</sup>	$2.0 \times 10^{-11}$	$2.0 \times 10^{-11}$	Ahn et al. (2008); Ikeda-Fukazawa (2004a, 2004b)
$D_w$	Diffusion coefficient of radon in water	m <sup>2</sup> s <sup>-1</sup>	$1.3 \times 10^{-9}$	$1.3 \times 10^{-9}$	Barrio-Parra et al. (2022)
$\eta$	Sum of the fractional emanation coefficients	-	0.2	0.2	Cozmuta et al. (2003)
$\lambda$	Decay constant of radon	s <sup>-1</sup>	$2.1 \times 10^{-6}$	$2.1 \times 10^{-6}$	Nazaroff (1992)
$C^{Ra226}$	Mean radium-226 activity per unit dry mass of subsoil	Bq kg <sup>-1</sup>	40	40	Cozmuta et al. (2003)

reduce by decay, while the other allows radon to exit the building. Boundaries within the building and between the soil and permafrost were set to represent continuity in radon concentration, and the soil surface boundary condition was  $C_a = 0$  Bq/m<sup>3</sup>. The former condition models unimpeded access of radon to the house through the soil but not through the water supply (Adinehvand et al., 2019; Bem et al., 2014), while the latter represents the normal exhalation of radon from soil. Boundaries between the soil or permafrost and the basement of the building were initially set to represent continuity in the radon concentration. This last assumption was made for simplicity. All models include 0.3 m thick basement walls whose boundaries represent radon concentration continuity, but whose porosity, diffusion coefficient, and gas permeability are taken from those of concrete (Cozmuta et al., 2003).

In this work, we have not considered second-order complications to the overall flow regime that may be caused by ground ice formation or thawing because we have not attempted to carry out modeling of seasonal changes. In addition, all modeled volumes are considered homogeneous.

## 2.4. Input Parameters

The input parameters modeled in the study are represented by Table 1. A major challenge has been to obtain values for porosity, diffusion coefficients, and gas permeability that are representative of reality. There have been very few experimental determinations of these parameters. A mean value of 0.245 has been assumed for the soil porosities, both before, during, and after partial thawing. This implies that there is no compaction concomitant upon thawing, which is a significant assumption of the modeling. The bulk density of the subsurface was calculated assuming the density of the matrix grains to be 2,650 kg/m<sup>3</sup>, which is the density of quartz. The Ostwald coefficient for the solution of radon in water is 0.253 at 293 K (Ongori et al., 2015), and that for the solution of radon in ice has been assumed to be the same. The sources of the remaining 11 input parameters are given in Table 1.

In all cases, the modeling began with the development of a steady-state concentration of radon throughout the model. In all cases, this led to an accumulation of radon behind the permafrost barrier and depletion of radon in the soil above the permafrost barrier. There is a quasi-linear increase in radon concentration with depth across the permafrost layer. This arises from the radon sources within the permafrost itself and is modeled at steady-state

(i.e., assuming that the permafrost has been in-place and undisturbed for long enough for a steady initial condition to be attained (Cong et al., 2022)).

Ideally modeling should be carried out on parameters whose mean and extreme values were known, and preferably whose spatiotemporal variabilities were also known. Unfortunately, there is an extreme sparsity of data for this modeling in the literature, most of which is included in this paper. It is clear that more accurate modeling will only be possible if significant fundamental research is put into measuring the statistical and spatiotemporal variabilities of the input parameters to this modeling.

Hence, in this work, we initially assume that the distributions of solute and the radiogenic capability of the soil are uniform irrespective of their frozen state and that any variability to these parameters is caused by temperature variations within the model (particularly with depth) is insignificant. This last assumption is particularly problematic because intuition informs us that saturations, radon concentrations, porosity, and diffusion coefficients will vary with temperature (Feng et al., 2021; Phong Thu et al., 2020). However, we simply do not have the experimental data on the variability of these parameters to incorporate them in our model.

The pore fluid pressures during modeling varied from 0.101325 MPa at the surface, which is the standard atmospheric pressure, to 0.698 MPa at 45 m depth with a 13 m thick impermeable permafrost layer at any depth. The maximum vertical pressure gradient is 0.0218 MPa/m, which is small, but capable of driving advective flow if the permeabilities of the permafrost become sufficiently low due to thawing.

## 2.5. Modeling Permafrost Thaw

No quantitative information exists concerning the variation of the effective diffusion coefficient of radon through permafrost as it thaws. However, the function representing how effective diffusion coefficient ( $D_{eff}$ ) varies with time ( $t$ ) during thawing is needed to model radon transport in all scenarios other than when permafrost thaws completely and instantaneously. We model the changes to the diffusion coefficient of radon through thawing permafrost by assuming that the effective diffusion coefficient ( $D_{eff}$ ) follows a generic exponential transition from the effective diffusion coefficient of the fully frozen permafrost ( $D_p$ ) to that of the fully thawed soil ( $D_s$ ) according to  $D_{eff} = D_s - (D_s - D_p)e^{-at}$ . Here  $t$  is the time in years and an exponential coefficient ( $a$ ), which has the units per year, controls the rate of change.

Figure 3 shows such thawing functions for seven different  $a$ -values varying from  $a = 0.001 \text{ year}^{-1}$  to  $a = 1,000 \text{ year}^{-1}$ . In this figure, we have used arbitrary units for diffusion coefficient for clarity, with the effective diffusion coefficient for the unthawed permafrost  $D_p = 1$  unit, and the effective diffusion coefficient for completely thawed soil being given by  $D_s = 1,000$  units. The solid curves show the scenarios used in this modeling, from quasi-instantaneous thawing represented by the black line ( $a = 1000 \text{ year}^{-1}$ ) for which there is a 40% thaw after 4.38 hr, to the longest transition represented by the orange line ( $a = 0.001 \text{ year}^{-1}$ ) for which there is a 40% thaw after 500 years). The curve colors are the same as used for the results in Figure 8. The dashed lines show scenarios that were not modeled in this paper.

It should be noted that the definition of porosity used in this work is the fraction of the bulk material which is not solid minerals. Hence thawing in the absence of compaction will increase the water saturation and decrease the ice fraction occupying the porosity.

We recognize that our permafrost thawing model is simplistic. In all cases, thawing has been applied uniformly to the whole permafrost layer. In reality, there may be a preferential distribution of permafrost degradation (starting at the top or the bottom of the permafrost layer). However, we feel that a more complex model is not justified in the absence of quantitative thawing data.

## 3. Results

### 3.1. Permafrost as a Radon Barrier

Here we present results from numerical modeling of radon transport through soil, permafrost, and various types of ventilated and unventilated model buildings. Modeling has been carried out for two types of building, for scenarios involving advective and/or diffusive transport, and for different rates of permafrost thawing.

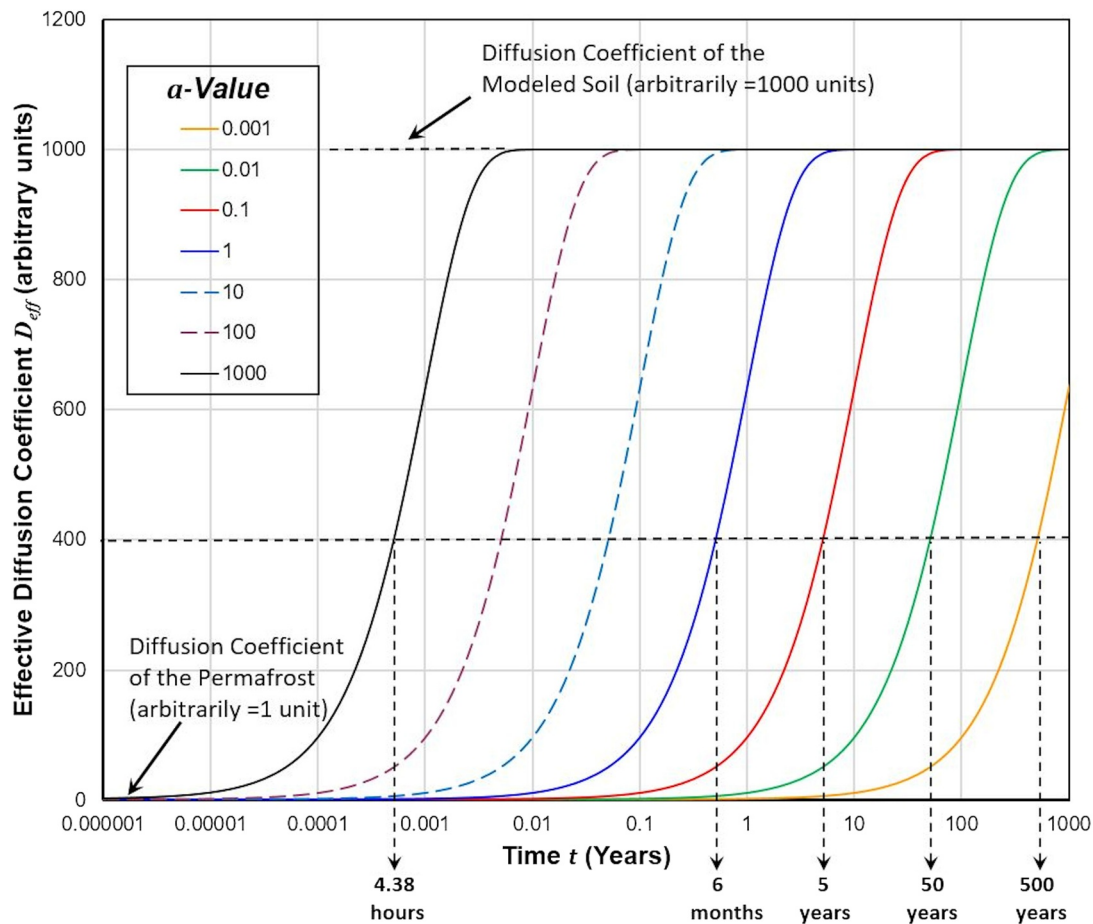


**Figure 3.** Modeled variation of the effective diffusion coefficient ( $D_{eff}$ ) for a partially thawed permafrost in arbitrary units as a function of time  $t$  in years from the effective diffusion coefficient of fully frozen permafrost ( $D_p = 1$  unit) to that of fully thawed soil ( $D_s = 1,000$  units) according to  $D_{eff} = D_s - (D_s - D_p) e^{-at}$ , where the exponent  $a$  controls the rate of change.

Figure 1 shows the three model scenarios that were studied in this work together with boundary conditions and a typical finite element modeling mesh.

Initial modeling was carried out with a 13 m thickness of permafrost in place and the modeling parameters are shown in Table 1. We find that the presence of the permafrost acts as an effective radon barrier even in the absence of advective transport. This is the case irrespective of how deep the permafrost barrier is placed, as shown in Figure 4 for the basement style building.

For the world average  $Ra^{226}$  activity of 39 Bq/kg (UNSCEAR, 2000), the permafrost reduces the domestic radon concentrations by 80%–90% (4–8 Bq/m<sup>3</sup>) while leading to an increase in the concentration in the radon behind the barrier by up to 11.43 times (445.8 Bq/m<sup>3</sup>). Consequently, permafrost can provide effective protection from radon.

This modeling observation accords well with the observations of Conen and Robertson (2002), who report a strong decrease in radon flux from a constant rate of about 1 atom cm<sup>-2</sup> s<sup>-1</sup> for all latitudes south of 30°N, decreasing northwards to 0.2 atom cm<sup>-2</sup> s<sup>-1</sup> at 70°N.

### 3.2. The Effect of Building Type

Thawing of the permafrost is beginning to occur as a result of global climate change (WHO, 2019; Witze, 2020; Yumashev et al., 2019). When we model this thaw we observe transient plumes of radon passing through some types of building. The plume of radon has an intensity and duration which depends on the style of building, the

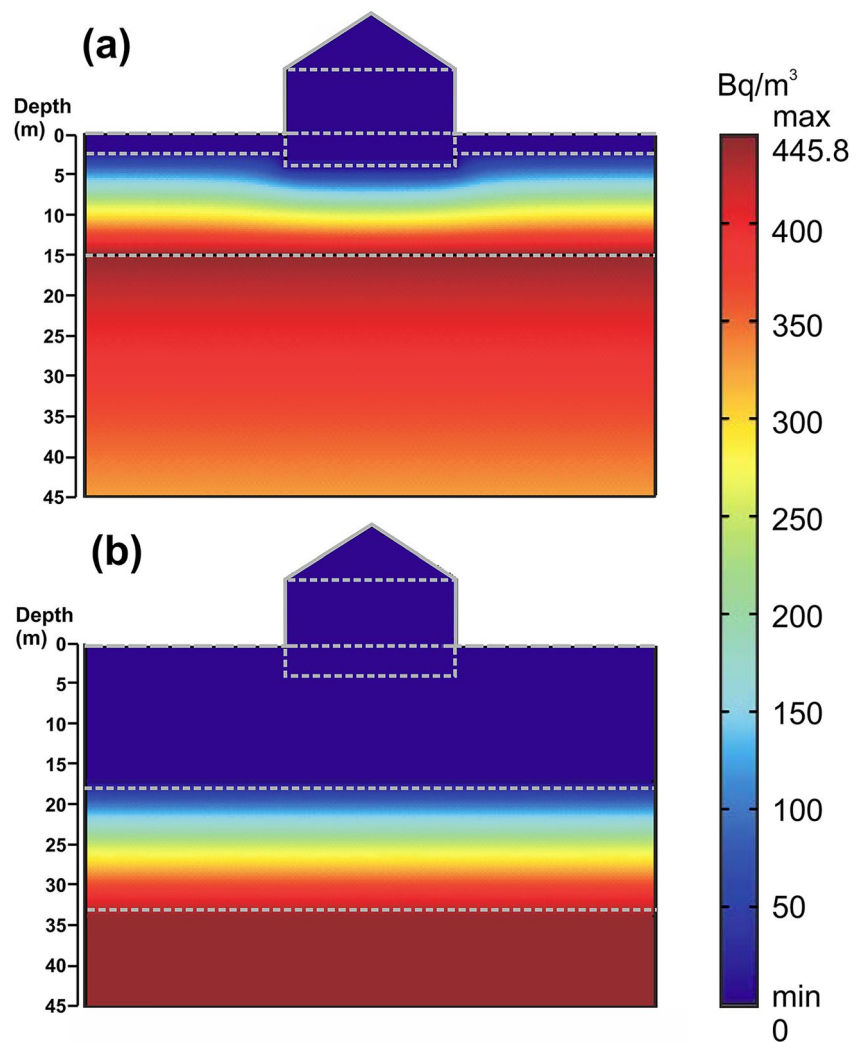


**Figure 4.** The initial steady-state distribution of radon concentration (in  $\text{Bq/m}^3$ ) with respect to the initial layer of permafrost. (a) Top of permafrost at 2 m depth; permafrost thickness 13 m. (b) Top of permafrost at 18 m depth; permafrost thickness 15 m.

depth to the permafrost layer, whether advection, as well as diffusion, plays a part in the radon transport process, and the time taken to thaw the permafrost sufficiently for it to become patent to radon.

For the type of building that contains a basement that is buried in the soil, we observe a well-developed plume of radon that lasts over a decade and is greater than the threshold value of  $200 \text{ Bq/m}^3$  for up to about 7 years Figure 5 shows the temporal variation of this observation as radiation maps for the building and the soil at 8 selected time-steps out of about 180 that resulted from the modeling. A video of the progression of the plume for all rendered time-steps is available by request from the author or from the supplementary dataset (Glover, 2022).

In this case, the depth to the top of the permafrost is 2 m and the thawing of the permafrost is considered to be quasi-instantaneous. The time step parts are shown on a restricted scale to show the radon plume more effectively. In these models, the initial values of radon concentration within the building ( $5\text{--}10 \text{ Bq/m}^3$ ) are increased transiently, up to 70-fold, to values of the order of about  $350 \text{ Bq/m}^3$  by the passage of the released radon through the building. After a number of years, the radon disperses and the value in the building falls to the value that would have been typical if the permafrost layer had not originally occurred (around  $39 \text{ Bq/m}^3$  in this modeling) over a period greater than 50 years.

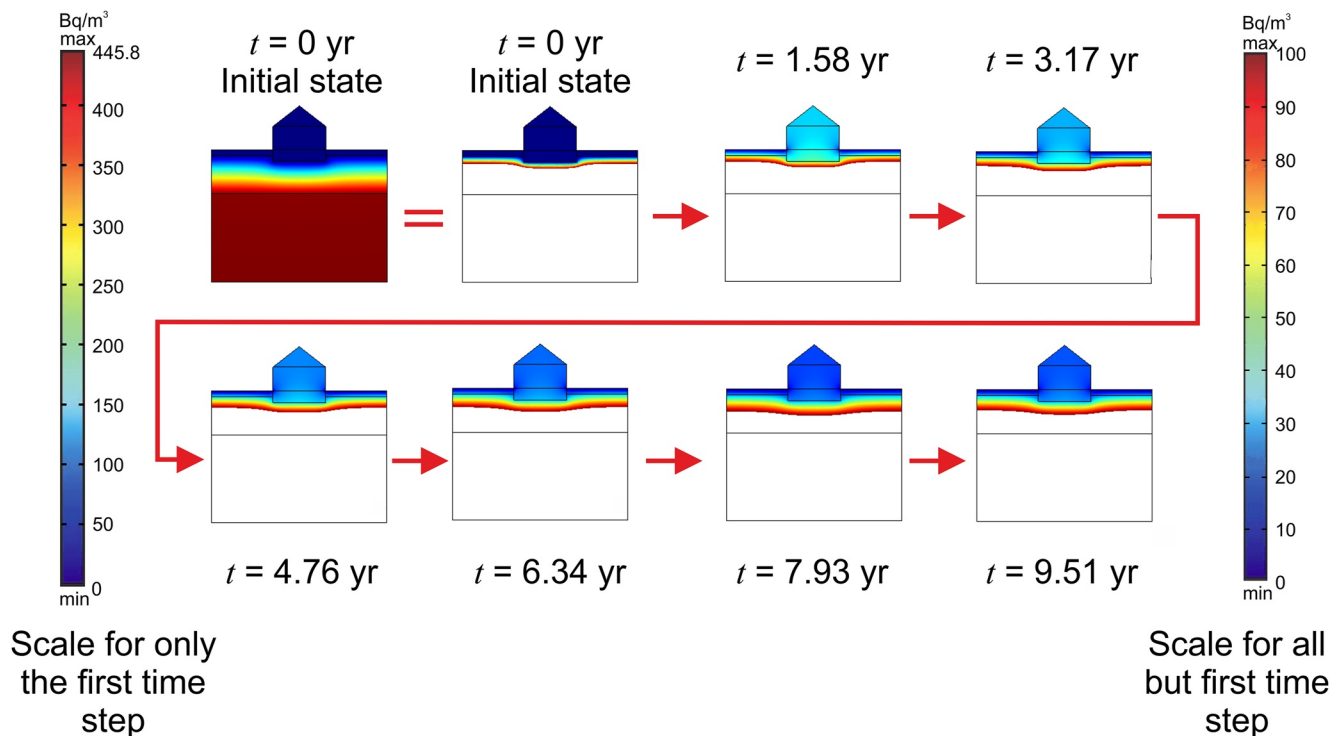


**Figure 5.** Selected time steps (from 180) showing the radon concentration plume passing through the buried basement-style model building after the quasi-instantaneous thawing of the permafrost (left scale for the top-right model, restricted right scale for all of the remaining time steps).

For a building having a basement that rests directly on the ground, we observed a temporal variation of the plume that is almost identical to that shown in Figure 5, and hence we do not include it as a separate figure. However, for buildings raised on piles, there was no increase in radon in the building for any of the scenarios. Figure 6 shows the analog temporal variation in this case. This expected result confirms that buildings built on piles are sufficiently well-ventilated that they do not suffer from radon build-up.

It is recognized that the common practice is for the spaces under pile-supported dwellings to be partially enclosed in order that the space can be used as a secure store and to alleviate the ingress of snow. We have not attempted to model this scenario, but we believe that it is unlikely for radon to build-up in these semi-ventilated spaces sufficiently for the insulated building above to see an increase in radon concentration.

### 3.3. The Effect of Permafrost Depth

The remainder of this paper address buildings with basements that either lie partly or immediately above or within the permafrost.

In the first of these scenarios, we modeled the mean intensity and transience of radon plumes within the building as a function of the depth of the buried permafrost layer for the case where all radon was transported by diffusion, which is the common case, and for a sudden increase of the ability of the permafrost to transport radon. Such an occurrence might be likened to instantaneous thawing, but in reality, is more likely to occur when sufficient thaw has occurred for a radon transport pathway to form.

The resulting data are given in the form of arithmetic mean radon concentration (in  $\text{Bq/m}^3$ ) within the building as a function of time so that the temporal progression of risk due to radon can be tracked more quantitatively and with a better temporal resolution.

Figure 7 shows that both the radon concentration and the period of raised radon concentrations within the building increase as the depth to the permafrost layer decreases. Radon concentrations do not exceed  $200 \text{ Bq/m}^3$  for permafrost layers starting at a depth greater than about 9 m. However, for permafrost starting at less than this

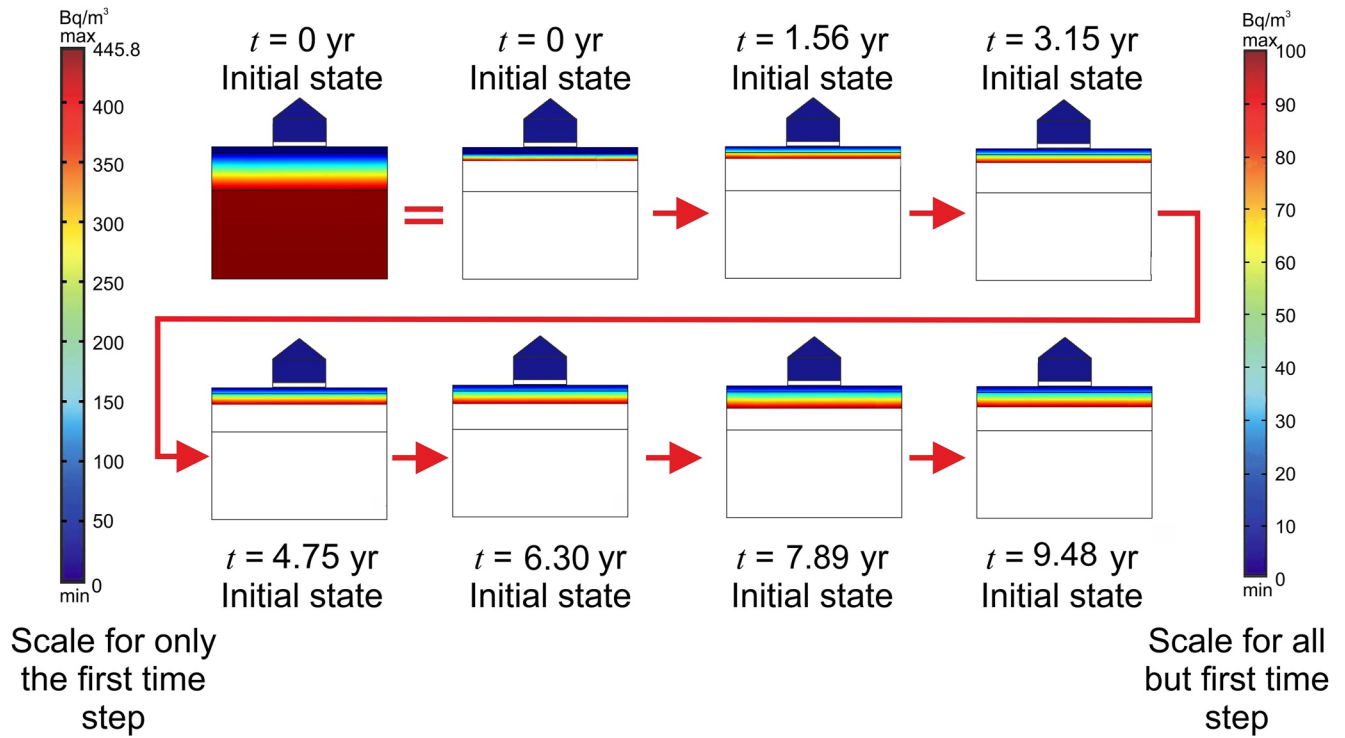


**Figure 6.** Selected time steps (from 180) showing the radon concentration plume passing through the piles-supported model building after the quasi-instantaneous thawing of the permafrost (left scale for the top-right model, restricted right scale for all of the remaining time steps).

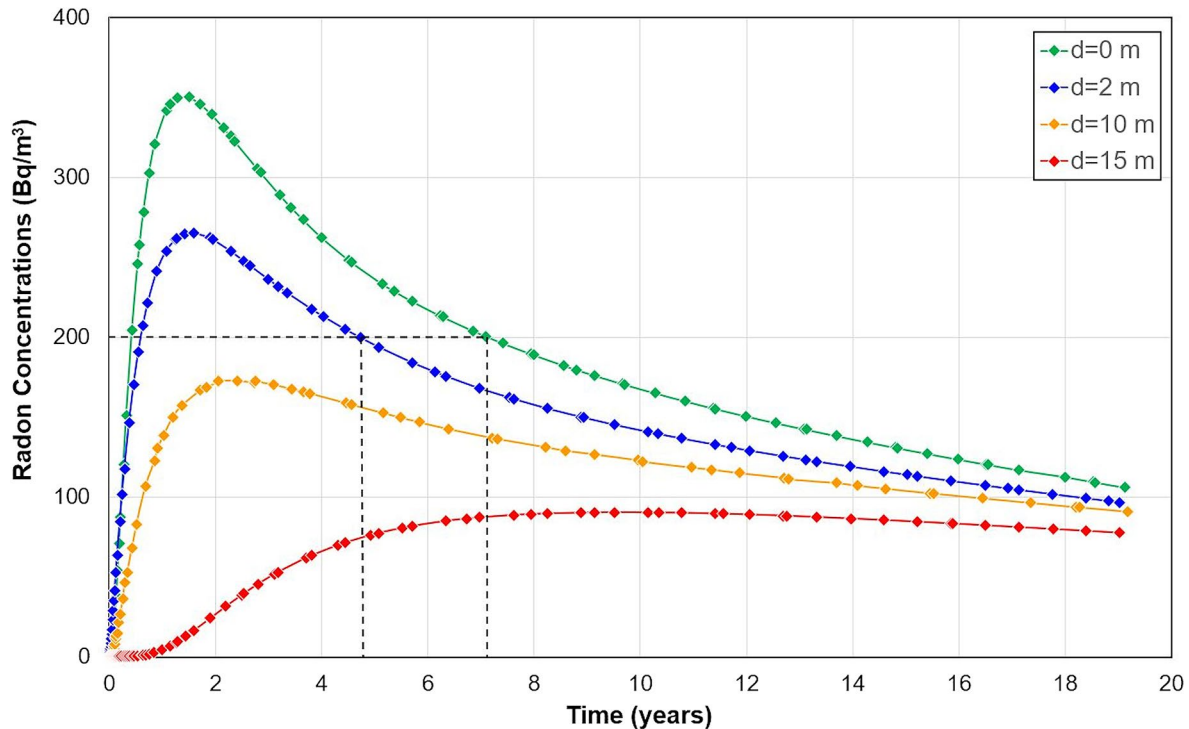


**Figure 7.** Evolution of arithmetic mean radon concentration within basement style buildings after a sudden increase in the ability of permafrost to transport radon by diffusion for four different depths to the upper surface of the permafrost ( $d = 0\text{--}15$  m).

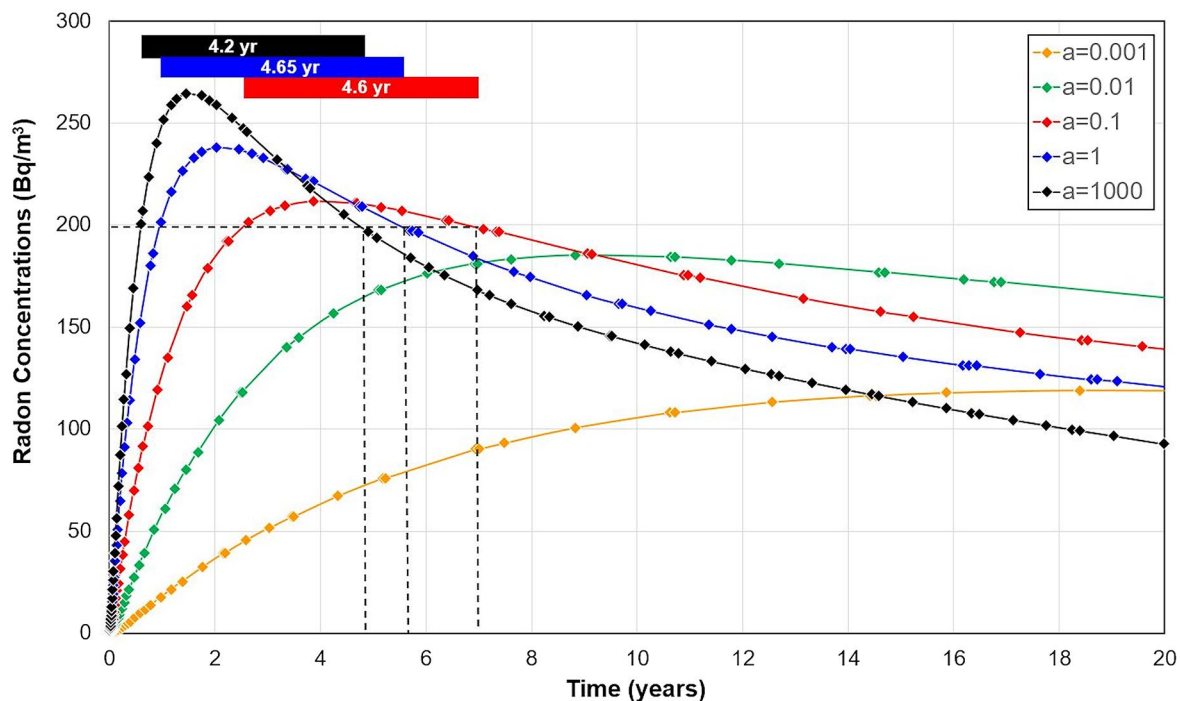


**Figure 8.** Evolution of the arithmetic mean radon concentration for quasi-instantaneous thaw and four longer thaw profiles approximating to 40% increase in diffusion coefficient after 0.5, 5, 50, and 500 years, as defined in the methodology, and  $d = 2$  m. Colored bars show time above the  $200 \text{ Bq/m}^3$  threshold.

depth, the plume of radon can exceed  $350 \text{ Bq/m}^3$  and remain over the  $200 \text{ Bq/m}^3$  level for over 6.66 years. The greater depths provide diffusive routes for the radon to disperse and be released to the atmosphere without encountering the building.

### 3.4. The Effect of Speed of Permafrost Thaw

The results in Figure 7 assume an instantaneous transition of the diffusion coefficient for radon from that for permafrost to that for the associated soil. Clearly, this assumption is unrealistic. Consequently, we have tested five scenarios where the change in the effective diffusion coefficient  $D_{eff}$  varies as a function of time as described in the methodology. In these scenarios a 40% increase in diffusion coefficient occurs after 0.5, 5, 50, and 500 years as controlled by an exponential coefficient  $a = 1, 0.1, 0.01,$  and  $0.001 \text{ year}^{-1}$ , respectively. The results of modeling are shown in Figure 8.

In all cases, the radon concentration peak diminishes and spreads out in time as the thawing process lengthens. It is expected that this occurs because the longer the timescale, the greater chance that the radon can diffuse laterally ‘missing’ the building, while the radon already in the building has a greater time to disperse naturally.

The  $200 \text{ Bq/m}^3$  threshold is exceeded for all scenarios where  $a < 0.035$ , which represents a change in effective diffusion coefficient  $D_{eff}$  of 40% in 15 years or shorter. Figure 8 shows the time for which the mean radon concentration in the building is above  $200 \text{ Bq/m}^3$  as colored bars. The period for which the radon concentration is greater than  $200 \text{ Bq/m}^3$  is 4.2 years for the quasi-instantaneous case (black, 40% change in the effective diffusion coefficient  $D_{eff}$  in 4.38 hr), compared to 4.65 years (blue) for a 40% change in  $D_{eff}$  in 6 months, and 4.6 years (red) for a 40% change in  $D_{eff}$  in 5 years. The longer it takes to reach a 40% change in effective diffusion coefficient, the lower the peak radon concentration, until about 15 years, whereupon the peak radon concentration never exceeds the  $200 \text{ Bq/m}^3$  threshold.

In reality, thawing is likely to take place in step with seasonal temperature changes, which makes this modeling a very much simplified model. However, it does show that even if the transport is solely diffusional, short time scale changes can lead to large changes in radon concentration in buildings.

### 3.5. Radon Transport Mechanisms

It is expected that radon transport will mainly occur by diffusion. However, there may be occasions where diffusion and advection occur concurrently. Initial modeling indicates that added advection brings the peak in the radon concentration forward in time and increases its value significantly, but also reduces the length of time values exceed the 200 Bq/m<sup>3</sup> threshold. The plume of radon passes more swiftly by being driven by advective flow and might bypass the building if the transport pathways around it are easier than through the building. There is also the possibility that radon dissolved in advectively driven water may add to the radon concentration in the building, however, this transport mechanism was not modeled explicitly in this work.

It is also expected that the speed of permafrost thawing will also have less effect for scenarios including significant advective transport. Once partial thawing of permafrost leads to the development of connected pathways capable of sustaining flow they are expected to become dominant, reducing the sealing capacity of the remaining permafrost layer and resulting in short duration, barometrically-driven (Perrier & Girault, 2013), high intensity radon plumes which could be extremely dangerous. Further modeling will be required to confirm the implications of advective-diffusive radon transport.

It is clear that further modeling is needed and an exploration of diffusive and advectively-driven radon transport will be the subject of a future paper.

## 4. Discussion

The modeling presented in this paper represents only an initial study. The headline conclusion is that the thawing of permafrost could expose a significant number of people to levels of radon in excess of the 200 Bq/m<sup>3</sup> threshold that many countries adopt.

We recognize five important qualifying issues to the main conclusion, some of which will reduce the impact of the results and some which amplify their importance.

First, all of the results discussed in this work are for unventilated buildings. Consequently, the results should all be considered to be worst-case scenarios.

Second, many of the northern communities will be protected simply because their dwellings are well ventilated by traditional design, being built clear of the ground on piles (Buijze & Wright, 2021). However, many of the more modern buildings are not constructed in this way, and one must also take account of modern commercial developments that are occupied by workers for the greater portion of the day.

Third, it is currently unclear how fast the permafrost thaws. One might expect, and we show by modeling in this paper, that longer thaw times mitigate against a sudden release of radon. However, not enough is known about the transport properties of permafrost to predict the development of its permeability as it degrades. It may not be true that a 40% partial thawing of the permafrost results in a proportional increase in radon transport, as has been found for building materials with different water contents (Fournier et al., 2005). Rather, it is perfectly possible that a 5% partial thawing of the permafrost might abruptly open fractures in the permafrost that would then act as radon superhighways.

Fourth, we have been forced to make a number of assumptions in the modeling, some of which can be removed in future modeling. One example of this is the imposition of seasonal variations in thawing, perhaps based on field observations. The largest uncertainty in this modeling is the very sparse data concerning the storage, transport, and partition of radon in water, gas, solid, and ice phases within the permafrost and how these change as the permafrost thaws. It is, consequently, a major recommendation of this work that experimental field and laboratory measurements are carried out to clarify this uncertainty.

Another assumption in the modeling is that there is no reduction of porosity upon thawing, which is to say that there is no compaction of the soil upon thawing. We know that such compaction does occur and is significant. Furthermore, such compaction amounts to a process whereby radon can be 'pumped' out of the ground by the compaction process. Consequently, the results presented in this paper may represent less risk than is actually present.

Finally, it is well recognized that radon-acquired lung cancer is 25.8 (+5.4/−4.5) times more prevalent in tobacco smokers than it is for non-smokers (Darby et al., 2005). This is especially important considering that the prevalence of smoking amongst the inhabitants of northern Canada and Greenland is approximately three times that of the global average of 21% (WHO, 2019). These populations would be very significantly sensitive to any release of radon that may occur as a result of permafrost thaw.

This study has a number of aspects that can be improved upon. The first concerns the accuracy of some of the input parameters, for example, the porosities and effective diffusion coefficients. Improved values of these parameters will only be available when experimental measurements from typical sub-Arctic permafrost are available.

The second is also associated with experimental measurements, but those used in the validation of modeling results. It is proposed that measurements of radon emanation are carried out at a small scale while partially thawing permafrost. Such experiments could be carried out in a highly controlled manner in the laboratory or in the field. Either way, such experimental verification of the modeling results presented in this work is necessary.

The third aspect concerns second-order processes which should be modeled in the future providing supporting data is available. An example is a link between water, gas, and ice fractions and changes in porosity that occur as thawing progresses. Compaction of the partially thawed permafrost during thawing not only changes input parameters, but can result in heterogeneous distributions of ice, water, and gas phases in the subsurface. Hence, thawing produces heterogeneous modeling fields where the spatiotemporal nature of the subsurface should ideally be modeled in full, providing supporting data becomes available.

Future models should also improve the way that the buildings and their foundations are modeled. Many buildings in the ACPR have concrete foundations, which commonly contain connected crack networks. These will enhance access of radon into the building compared with the scenario modeled in this paper, which considers only the porosity, diffusion coefficient, and gas permeability of concrete. Furthermore, it is likely that large migration channels will develop in the permafrost and soil under foundations due to the migration of radon and redistribution of soil stresses. Hence a higher permeability in the soil and permafrost directly under the building would be indicated in future modeling.

## 5. Conclusions

We have used finite element modeling to examine the effect of permafrost thaw due to climate change on radon exposure in buildings.

Initial modeling showed that a layer of permafrost provides an effective barrier to radon irrespective of whether the permafrost starts near the surface or starts at depths up to 15 m, with radon concentrations behind the barrier reaching up to 445.8 Bq/m<sup>3</sup> which is almost 12 times the value that would have been the case without the presence of the barrier. This represents a dynamic reservoir of radon if it were released.

It was confirmed that increases in the ability of gases to diffuse through permafrost caused by instantaneous partial thawing resulted in the release of radon in a plume that raised the radon concentration in basement style buildings (either buried basements or basements resting on the surface) up to 350 Bq/m<sup>3</sup> and remaining greater than the 200 Bq/m<sup>3</sup> threshold for about 7 years for permafrost starting at the surface. Plumes were less intense and exceeded the threshold for shorter times as the depth to the top of the permafrost increased until the peak radiation of the plumes was no longer exceeding the threshold.

Pile-constructed buildings exhibited no rise in radon at any time in the modeling.

Modeling was carried out to take into account that thawing of permafrost will not be instantaneous. Thawing curves for the quasi-instantaneous case, and 40% thawing occurring in 0.5, 5, 50, and 500 years were examined. For the first three of these cases, the radon plume provided domestic radon concentrations greater than the 200 Bq/m<sup>3</sup> threshold for between 4.2 and 4.65 years, but later values did not exceed the threshold, with the threshold limit occurring at about 15 years for a 40% thaw.

Further modeling is being carried out to ascertain the effect of adding advective radon transport to the diffusion transport reported in this work, as well as to examine diurnal and seasonal thawing of the permafrost. Future modeling will also need to take account of a range of processes that may affect the outcomes. These include changes

in soil porosity and saturations due to compaction, changes in effective diffusion coefficients due to changes in temperature, and heterogeneous ice distributions.

We recognize that despite the problem of radon being allayed by good ventilation, the risk to the 5 million people who live on permafrost in the Arctic Circumpolar Permafrost Region is high because (a) rocks underlying these regions provide more radon than the global average, (b) radon has not previously been recognized as a problem in these areas due to the protective permafrost barrier, (c) northern populations have smoking rates that are about three times the global mean and that radon-acquired lung cancer is 25.8 (+5.4/-4.5) times more prevalent in tobacco smokers than it is for non-smokers, and (d) though traditional pile-constructed buildings still exist, more and more concrete basement-type buildings for homes, offices, shops, and industry are being built.

## Data Availability Statement

Data to produce all the plot figures supported by videos of model results and copies of every figure can be obtained from <https://doi.org/10.5281/zenodo.5833919>.

## References

- Alinehvand, K., Azadbakht, B., & Fallahi Yekta, M. (2019). Dose assessment and measurement of radon concentration in water supplies of Borujerd County in Iran. *International Journal of Radiation Research*, *17*(3), 507–511.
- Ahn, J., Headly, M., Wahlen, M., Brook, E. J., Mayewski, P. A., & Taylor, K. C. (2008). CO<sub>2</sub> diffusion in polar ice: Observations from naturally formed CO<sub>2</sub> spikes in the Siple Dome (Antarctica) ice core. *Journal of Glaciology*, *54*(187), 685–695.
- Al-Zoughool, M., & Krewski, D. (2009). Health effects of radon: A review of the literature. *International Journal of Radiation Biology*, *85*(1), 57–69.
- Barrio-Parra, F., Hidalgo, A., Izquierdo-Díaz, M., Arévalo-Lomas, L., & De Miguel, E. (2022). *1D-RnDPM: A freely available 222Rn production, diffusion, and partition model to evaluate confounding factors in the radon-deficit technique* (p. 807). Science of the Total Environment. BEIR VI. (1999). *Biological effects of ionizing radiation VI report. Health effects of exposure to indoor radon*. National Academy Press.
- Bem, H., Plota, U., Staniszevska, M., Bem, E. M., & Mazurek, D. (2014). Radon (222Rn) in underground drinking water supplies of the Southern Greater Poland Region. *Journal of Radioanalytical and Nuclear Chemistry*, *299*(3), 1307–1312.
- Bjerregaard, P., Mulvad, G., & Pedersen, H. S. (1997). Cardiovascular risk factors in Inuit of Greenland. *International Journal of Epidemiology*, *26*(6), 1182–1190.
- Buijze, J. A. J. C., & Wright, A. J. (2021). The potential for the passive house standard in Longyearbyen – The high arctic. *Building Services Engineering Research and Technology*, *42*(3), 307–325.
- Chen, C., Thomas, D. M., & Green, R. E. (1995). Modeling of radon transport in unsaturated soil. *Journal of Geophysical Research*, *100*(B8), 15517–15525.
- Chung, L. K., Mata, L. A., Carmona, M. A., Shubayr, N. A. M., Zhou, Q., Ye, Y., & Kearfott, K. J. (2020). Radon kinetics in a natural indoor radon chamber. *The Science of the Total Environment*, *734*, 139167.
- Chuvilin, E., Grebenkin, S., & Zhmaev, M. (2021). Gas permeability of sandy sediments: Effects of phase changes in pore ice and gas hydrates. *Energy and Fuels*, *35*(9), 7874–7882.
- Conen, F., & Robertson, L. B. (2002). Latitudinal distribution of radon-222 flux from continents. *Tellus Series B Chemical and Physical Meteorology*, *54*(2), 127–133.
- Cong, J., Gao, C., Xing, W., Han, D., Li, Y., & Wang, G. (2022). Historical chemical stability of carbon pool in permafrost peatlands in northern Great Khingan Mountains (China) during the last millennium, and its palaeoenvironmental implications. *Catena*, *209*. <https://doi.org/10.1016/j.catena.2021.105853>
- Cozmata, I., van der Graaf, E. R., & de Meijer, R. J. (2003). Moisture dependence of radon transport in Concrete: Measurements and modeling. *Health Physics*, *85*(4), 438–456.
- Darby, S., Hill, D., Auvinen, A., Barros-Dios, J. M., Baysson, H., Bochicchio, F., et al. (2005). Radon in homes and risk of lung cancer: Collaborative analysis of individual data from 13 European case-control studies. *BMJ*, *330*(7485), 223–227.
- Darby, S., Hill, D., Deo, H., Auvinen, A., Barros-Dios, J. M., Baysson, H., et al. (2006). Residential radon and lung cancer - Detailed results of a collaborative analysis of individual data on 7148 persons with lung cancer and 14208 persons without lung cancer from 13 epidemiologic studies in Europe. *Scandinavian Journal of Work, Environment and Health Supplement*, *32*(1), 1–84.
- Dela Cruz, C. S., Tanoue, L. T., & Matthay, R. A. (2011). Lung cancer: Epidemiology, etiology, and prevention. *Clinics in Chest Medicine*, *32*(4), 605–644.
- Eichler, B., Zimmermann, H. P., & Gäggeler, H. W. (2000). Adsorption of radon on ice surfaces. *The Journal of Physical Chemistry A*, *104*, 3126–3131.
- Evans, R., Dal Poghetto, G., Nilsson, M., & Morris, G. A. (2018). Improving the interpretation of small molecule diffusion coefficients. *Analytical Chemistry*, *90*, 3987–3994.
- Feng, S., Li, C., Cui, Y., Ye, Y., Li, X., Liu, Y., et al. (2021). Novel method for measuring temperature-dependent diffusion coefficient of radon in porous media. *Applied Radiation and Isotopes*, *169*, 091506. <https://doi.org/10.1016/j.apradiso.2020.109506>
- Fortin, G., Van Bochove, E., Jones, H. G., Thériault, G., & Bernier, M. (2007). The simultaneous determination of air permeability and gas diffusion through ice layers in the field. *Nordic Hydrology*, *38*(3), 203–210.
- Fournier, F., Groetz, J., Jacob, M., Crolet, J. M., & Lettner, J. M. (2005). Simulation of radon transport through building materials: Influence of the water content on radon exhalation rate. *Transport in Porous Media*, *59*(2), 197–214.
- Gadd, M. S., & Borak, T. B. (1995). In-situ determination of the diffusion coefficient <sup>222</sup>Rn in concrete. *Health Physics*, *68*(6), 817–822.
- Glover, P. W. J. (2022). Increased radon exposure from thawing of permafrost due to climate change – Supplemental data. *Zenodo*. <https://doi.org/10.5281/zenodo.5833919>
- Ikedda-Fukazawa, T., Kawamura, K., & Hondoh, T. (2004a). Diffusion of nitrogen gas in ice Ih. *Chemical Physics Letters*, *385*(5–6), 467–471.

- Ikeda-Fukazawa, T., Kawamura, K., & Hondoh, T. (2004b). Mechanism of molecular diffusion in ice crystals. *Molecular Simulation*, *30*(13–15), 973–979.
- Krewski, D., Lubin, J. H., Zielinski, J. M., Alavanja, M., Catalan, V. S., Field, R. W., et al. (2005). Residential radon and risk of lung cancer: A combined analysis of 7 north American case-control studies. *Epidemiology*, *16*(2), 137–145.
- Krewski, D., Lubin, J. H., Zielinski, J. M., Alavanja, M., Catalan, V. S., Field, R. W., et al. (2006). A combined analysis of north American case-control studies of residential radon and lung cancer. *Journal of Toxicology and Environmental Health Part A*, *69*(7–8), 533–597.
- Lubin, J. H., Wang, Z. Y., Boice, J. D., Xu, Z. Y., Blot, W. J., De Wang, L., & Kleinerman, R. A. (2004). Risk of lung cancer and residential radon in China: Pooled results of two studies. *International Journal of Cancer*, *109*(1), 132–137.
- Moldrup, P., Olesen, T., Schjonning, P., Yamaguchi, T., & Rolston, D. E. (2000). Predicting the gas diffusion coefficient in undisturbed soil from soil water characteristics. *Soil Science Society of America Journal*, *64*, 94–100.
- Nazaroff, W. (1992). Radon transport from soil to air. *Reviews of Geophysics*, *30*, 137–160.
- Nitzbon, J., Westermann, S., Langer, M., Martin, L. C. P., Strauss, J., Laboor, S., & Boike, J. (2020). Fast response of cold ice-rich permafrost in northeast Siberia to a warming climate. *Nature Communications*, *11*(1), 2201.
- Ongori, J. N., Lindsay, R., & Mvelase, M. J. (2015). Radon transfer velocity at the water-air interface. *Applied Radiation and Isotopes*, *105*, 144–149.
- Othman, N. D., Rashid, A. S. A., Hashim, S., Sanusi, M. S. M., & Bery, A. (2021). Radon gas migration through soil – A review. *Journal of Mines, Metals and Fuels*, *69*(8), 3–8.
- Pawel, D. J., & Puskin, J. S. (2003). *EPA assessment of risks from radon in homes*. United States Environmental Protection Agency Report. EPA 402-R-03-003.
- Peng, X., Zhang, T., Frauenfeld, O. W., Du, R., Jin, H., & Mu, C. (2021). A holistic assessment of 1979–2016 global cryospheric extent. *Earth's Future*, *9*(8), e2020EF001969. <https://doi.org/10.1029/2020EF001969>
- Perrier, F., & Girault, F. (2013). Harmonic response of soil radon-222 flux and concentration induced by barometric oscillations. *Geophysical Journal International*, *195*(2), 945–971.
- Peto, J., & Darby, S. (1994). Radon risk reassessed. *Nature*, *368*(6467), 97–98.
- Petrov, O., & Pubellier, M. (2018). *Tectonic map of the Arctic*. Commission for the geologic map of the world CGMW-VSEGEI.
- Phong Thu, H. N., Van Thang, N., & Hao, L. C. (2020). The effects of some soil characteristics on radon emanation and diffusion. *Journal of Environmental Radioactivity*, *216*, 106189. <https://doi.org/10.1016/j.jenvrad.2020.106189>
- Ramage, J., Jungsberg, L., Wang, S., Westermann, S., Lantuit, H., & Heleniak, T. (2021). Population living on permafrost in the Arctic. *Population and Environment*, *43*(1), 22–38.
- Rogers, V. C., & Nielson, K. K. (1991a). Multiphase radon generation and transport in porous material. *Health Physics*, *60*(6), 807–815.
- Rogers, V. C., & Nielson, K. K. (1991b). Correlations for predicting air permeabilities and <sup>222</sup>Rn diffusion coefficients of soils. *Health Physics*, *61*(2), 225–230.
- Scheib, C., Appleton, J. D., Miles, J. C. H., Green, B. M. R., Barlow, T. S., & Jones, D. G. (2009). Geological controls on radon potential in Scotland. *Scottish Journal of Geology*, *45*(2), 147–160.
- Turetsky, M. R., Abbott, B. W., Jones, M. C., Anthony, K. W., Olefeldt, D., Schuur, E. A. G., et al. (2020). Carbon release through abrupt permafrost thaw. *Nature Geoscience*, *13*(2), 138–143.
- UNSCEAR. (2000). *United Nations Scientific Committee on the effects of atomic radiation. Sources and effects of Ionizing radiation. UNSCEAR 2000 report to the general Assembly*. with Scientific Annexes.
- WHO. (2009). In H. Zeeb, & F. Shannoun (Eds.), *WHO Handbook on Indoor radon, A Public health Perspective*. World Health Organisation.
- WHO. (2019). *WHO global report on trends in prevalence of tobacco use 2000–2025* (3rd ed.). World Health Organization.
- Witze, A. (2020). The Arctic is burning like never before - And that's bad news for climate change. *Nature*, *585*(7825), 336–337.
- Worsley, P. (1986). Palaeoclimate: Permafrost and ice-wedge growth. *Nature*, *322*, 683–684.
- Yumashev, D., Hope, C., Schaefer, K., Riemann-Campe, K., Iglesias-Suarez, F., Jafarov, E., et al. (2019). Climate policy implications of nonlinear decline of Arctic land permafrost and other cryosphere elements. *Nature Communications*, *10*(1), 1900.